Structure and Dynamics of Ribonuclease A During Thermal Unfolding: The Failure of the Zimm Model

Jennifer Fischer[†‡], Aurel Radulescu[¶], Peter Falus[§], Dieter Richter[†], Ralf Biehl[*†‡],

[†] Jülich Centre for Neutron Science (JCNS-1) and Institute of Biological Information Processing (IBI-8), Forschungszentrum Jülich GmbH, 52425 Jülich, Germany

[¶]Jülich Centre for Neutron Science JCNS at Heinz Maier-Leibnitz Zentrum (MLZ), Forschungszentrum Jülich, 85748 Garching, Germany

[§]Institut Laue-Langevin (ILL), 71 rue des Martyrs, 38042 Grenoble, Cedex 9, France

KEYWORDS disordered protein, Arrhenius, ZIF, internal friction, dynamics, neutron spin echo spectroscopy

ABSTRACT: Disordered regions as found in intrinsically disordered proteins (IDP) or during protein folding define response time to stimuli and protein folding times. Neutron spin echo Spectroscopy is a powerful tool to access directly collective motions of the unfolded chain to enlighten the physical origin of basic conformational relaxations. During thermal unfolding of native Ribonuclease A we examine structure and dynamics of the disordered state within a two-state transition model using polymer models including internal friction to describe the chain dynamics. The presence of 4 disulfide bonds alters the disordered configuration to a more compact configuration compared to a Gaussian chain that is defined by the additional links as demonstrated by coarse grained simulation. The dynamics of the disordered chain is described by Zimm dynamics with internal friction (ZIF) between neighboring amino acids. Relaxation times are dominated by mode independent internal friction. Internal friction relaxation times show an Arrhenius like behavior with an activation energy of 33 kJ/mol. The Zimm dynamics is dominated by internal friction and suggest that the characteristic motions correspond to overdamped elastic modes similar to motions observed for folded proteins but within a pool of disordered configurations spanning configurational space. For IDP internal friction dominates while solvent friction and hydrodynamic interactions are smaller corrections.

INTRODUCTION

The structure-function paradigm postulated by Fischer relates the microscopic structure of proteins to their function[1]. One class of proteins contradict the structure-function theorem fundamentally, the so called intrinsically disordered proteins (IDP's) sometimes also termed natively unfolded proteins. Although IDP's have a lack of secondary and tertiary structure they are functional[2,3]. The biological role of intrinsic disorder is focused on proteins important for cell signaling, transcription, and chromatin remodeling functions[4]. Disordered regions in proteins serve as flexible links connecting folded domains or adjoin folded domains allowing ligand binding or regulation of self assembly[2]. Many IDP's fold upon binding to the ligand, whereby a large ligand surface area can be buried[5]. Additionally, the folding process as transition from a disordered/unfolded state to a folded functional configuration is important to understand protein synthesis[6]. Very little is known about the dynamics of the disordered state and the physical origin of chain relaxation. In particular the dynamics during folding/unfolding of a native folded protein is difficult to access as it is not an equilibrium process. On the other hand, IDP should show the same dynamic characteristics in an equilibrium state.

Protein folding/unfolding is often described as a transition between a folded and unfolded state within a simple two state picture assuming a cooperative folding process. This is questioned meanwhile by multi step processes with intermediate states or continuum transitions right up to downhill/uphill (un)folding[7]. The kinetics of the transition is not only related to the energetic barrier but also to the diffusion in the energy landscape with contribution from friction with the solvent and friction within the molecule (internal friction). Thermodynamic kinetic measurements of unfolding by e.g. tryptophan fluorescence or laser induced T-jump experiments have been used to relate unfolding kinetics to solvent viscosity within Kramers theory in the high viscosity limit [8–12]. Additional osmolytes in the solvent reveal the contribution of internal friction in the polypeptide chain as an additional term to viscosity.

A direct access to measure conformational flexibility is challenging for structural analysis, but the dynamics are expected to resemble the dynamics observed for polymers as Rouse or Zimm dynamics[13] and were accessed by Förster resonance energy transfer combined with nanosecond fluorescence correlation spectroscopy (FRET/nsFCS), nuclear magnetic resonance (NMR), neutron spin echo spectroscopy (NSE) or MD simulations[11,14–17]. While FRET/nsFCS accesses only the dynamics between specific labels, NMR is sensitive for bond vectors on an atomic scale. NSE is settled in between as it is perceptive for collective motions on several nanometer length- and nanosecond timescale of native proteins assessing amplitude and relaxation times. NSE

needs no labels or osmolytes to discern friction with the solvent from internal friction.

In this work, the structure and dynamics of native and unfolded Ribonuclease A (RNase) and the transition between these states during thermal unfolding is investigated. RNase is a saddle-shaped protein with 4 disulfide bonds that cleaves RNA and has a long four-stranded antiparallel β-sheet region and 3 short α-helices (see Figure 1). It is a very stable protein that was used extensively for studying protein folding and unfolding as it refolds into its native configuration[18]. The aim of this work is to gain new insights into protein folding/unfolding dynamics and dynamics of amino acid chains that are closely related to the function of intrinsically disordered proteins. The combination of small angle neutron and X-ray scattering (SANS/SAXS) together with neutron spin echo spectroscopy (NSE) provides a unique tool to study the large-scale collective dynamics of proteins to explore the role of internal friction onto dynamics of an unfolded protein chain.

METHODS

Sample preparation

Ribonuclease A (Rnase) was purchased from Sigma Aldrich, dissolved in D_2O buffer and filtered with a 300kDa MW cutoff spin filter to remove aggregates. The buffer was 10 mM potassium phosphate with 100mM NaCl, 99.9 D_2O with respective $H_nK_{3-n}PO_4$ ratio to result in specific pH. Final pH was adjusted by titration with DCl or NaOD. For neutron scattering experiments the samples were dialyzed for 24h to allow H/D exchange of the proteins. The dialysate was used in the experiments for the background measurement with the same H/D content. Protein concentration was determined by optical absorption at 280 nm with an extinction coefficient of $E_{1\%} = 7$. Given pH values refer to pH-meter readings while the actual pD is 0.4 higher[19].

Circular dichroism and dynamic light scattering

Circular dichroism was measured on a J-810 spectropolarimeter (JASCO, Tokyo, Japan). The samples were measured in 0.1 mm thick quartz cuvettes under constant nitrogen flow at a concentration of 1 mg/ml between 187 – 250 nm. Spectra were measured 20 times, averaged and background corrected. Spectra were analyzed using the CDPro software taking the average of the algorithms CONTIN, SELCON3 and CDSSTR[20]. Dynamic light scattering was measured on a Zetasizer Nano ZS instrument (Malvern Instruments, Malvern, United Kingdom). Autocorrelation functions were analyzed by the included CONTIN like algorithm[21]. The hydrodynamic radius R_h was determined according to $R_h=k_BT/(6\pi\eta D)$ with the respective D_2O buffer viscosity and extrapolated to zero concentration to reach infinite dilution limit without influence of protein interaction on R_h.

Small angle scattering

SAXS was measured on X33 beamline at the EMBL, Hamburg[22]. The X-ray wavelength was 1.5 Å. Protein concentrations of 2.45 to 50.9 mg/ml were measured. SANS was measured on KWS-2 at the MLZ in Garching[23]. The neutron wavelength was 5 Å with a wavelength spread of 20%. Protein concentrations were 2.5, 5.0, 10.1 and 49.5 mg/ml. The scattering vector q is defined as $Q=4\pi/\lambda\cdot\sin(\theta/2)$ with the incident X-ray or neutron wavelength λ and the scattering angle θ. The measured background corrected and concentration scaled intensities I(Q) were linearly extrapolated to infinite dilution to extract the form factor P(Q). The structure factor S(Q) was extracted using the relation $I_c(Q) = cS(Q)P(Q)$ with the concentration c. Structural modelling of SANS data includes resolution smearing according to Pedersen[24].

Neutron spin echo spectroscopy

NSE was measured on NSE instrument IN15 at the ILL, Grenoble. Five incident neutron wavelengths with 6, 8, 9, 10 and 12 Å and wavelength spread of 20% were used. The area detector was sliced in 3 sections that each detector image results in 3 Q values. Respective buffer background measurements at 20°C were conducted and subtracted using the instrument software. The sample concentration was 51.1 mg/ml.

Software

SANS data were reduced to absolute intensity with the program QtiKWS provided by JCNS[25]. SAXS data were reduced to absolute intensity by the instrument software based on ATSAS[26]. Any further analysis as fitting , structure factor and hydrodynamic function evaluation was done using Jscatter[27]. Atomic modeling of PDB structures calculating formfactors was done by homemade routines (JscatterP) based on MMTK[28].

Rigid protein dynamics

NSE measures temporal and spatial correlations of molecular items expressed in the intermediate scattering function (ISF) $I(Q,\tau)/I(Q,0)$. At lower Q (SANS regime) the ISF is predominantly coherent scattering and large scale collective dynamics as translational and rotational diffusion but also internal dynamics as domain motions or dynamics of unfolded chains is observed for proteins[15,17,29]. Folded proteins with no internal dynamics show only contributions from translational and rotational diffusion D_t and D_r[30]

$$\frac{I(Q,t)}{I(Q,0)} = A_0 e^{-Q^2 D_t \tau} \sum_{l=0..\infty} S_l(Q) e^{-l(l+1)D_r\tau} / \sum_{l=0..\infty} S_l(Q)$$

$$S_l(Q) = \sum_m \left|\sum_i b_i\, j_l(Qr_i) Y_{l,m}(\Omega_i)\right|^2 \qquad 1$$

The effective diffusion in the initial slope can accordingly be calculated as

$$D_{eff}(Q) = D_t + \sum_{l=0..\infty} S_l(Q) l(l+1) D_r \qquad 2$$

$S_l(Q)$ are the terms of a multipole expansion with scattering length b_i of the atom i at position r_i and orientation $\boldsymbol{\Omega}_i$, $j_l(Qr_i)$ are the spherical Bessel functions and $Y_{l,m}$ the spherical harmonics. A_0 is an amplitude factor which is close to 1.

The diffusion of a nonspherical object is in general described by a 6x6 matrix with contributions from translational diffusion $\mathbf{D}_{t,3x3}$ and rotational diffusion $\mathbf{D}_{r,3x3}$ and off-diagonal elements $\mathbf{D}_{rt,3x3}=\mathbf{D}^T_{tr,3x3}$ describing rotational-translational coupling. The 6x6 matrix can be calculated based on the protein structure using the program HYDROPRO[31]. Using a scalar representation in equ. 1 e.g. $D_{r0}=\text{trace}(\mathbf{D}_{r,3x3})/3$ slightly overestimates the rotational contribution as the decoupling approximation is not exact[32].

Single particle translational diffusion D_t is modulated for finite concentrations as $D_t=D_{t0}H(Q)/S(Q)$ with D_{t0} as translational diffusion at infinite dilution. The structure factor S(Q) is related to direct interactions and hydrodynamic interactions are comprised in the hydrodynamic function H(Q)[33–35]. Using a structure factor extracted from experimental data implicitly includes the correction for anisotropy of particle shape according to Kotlarchyk[36]. Rotational diffusion is reduced by hydrodynamic interactions as $D_r=D_{r0}H_r$ where H_r can be estimated for hard spheres[32] as $1-H_r\approx(1-H_t(Q\to\infty))/3$. $H_\infty=H_t(Q\to\infty)$ is related to the change in viscosity as $H_\infty=\boldsymbol{\eta}_0/\boldsymbol{\eta}$ with buffer viscosity $\boldsymbol{\eta}_0$ and protein solution viscosity dependent on concentration $\boldsymbol{\eta}$[37,38].

Hydrodynamic Function

The hydrodynamic function H(Q) can be calculated for hard spheres from the known (measured) structure factor S(Q) using the $\delta\gamma$-expansion by[38,39]

$$H(Q) = H_\infty(\Phi) + \frac{3}{2\pi}\int_0^\infty d(Rq)\left(\frac{\sin(Rq)}{Rq}\right)^2 \left(1+\Phi S_{\gamma 0}(Rq)\right)^{-1} \times \int_{-1}^{1}(1-\cos(Q-q)^2) S(|Q-q|-1) \qquad 3$$

with the volume fraction Φ and the sphere radius R which is for hard spheres equivalent to the hydrodynamic radius. H_∞ is related to the short time self-diffusion coefficient D_s as $H_\infty(\Phi)=D_s(\Phi)/D_{t0}$ which is related to the intrinsic viscosity[38]. The function $S_{\gamma 0}(Q)$ is described in detail by Genz et al[39]. As a rule of thumb for the hydrodynamic function of hard spheres one might use for small volume fractions $H(Q)-H(\infty)=(S(Q)-1)/2$ which reflects the same modulation as found in S(Q) and leads to a compensation of the 1/S(Q) contribution.

To account for asymmetry in shape, internal flexibility or softness of the particle/protein that reduces the hydrodynamic interaction we may allow in a first order approximation that the hydrodynamic radius is reduced compared to a geometrical radius $R\to R_{eff}$. This allows to describe hydrodynamic interactions in the transition from a hard sphere to flexible proteins or soft polymer coils. In the limit of a small radius

R_{eff} the second term in equ 3 vanishes and we find $H(Q)=H_\infty(\Phi)$. An estimate for R_{eff} can be calculated from viscosity measurements fixing $H_\infty(\Phi)$ and the measured structure factor S(Q) and DLS measurements of the translational diffusion D_t at finite concentration and the infinite dilution limit D_{t0}.

Chain dynamics with hydrodynamic interaction and internal friction

A disordered protein chain can be described within a coarse-grained description of the dynamics of polymers in solution including hydrodynamic interactions known as the Zimm model[13]. A finite chain consists of *N* connected beads, separated by linear springs of length l. Each bead is exposed to friction with the solvent ξ_s , a restoring force from the springs connected to next neighbors κ and thermal random forces. To include internal friction ξ_{int} each bead exerts friction to its neighbors complementing the Zimm with internal friction model (ZIF)[40].

$$I(q,t) = \frac{exp(-q^2 D_{Zimm}\tau)}{N}\sum_{n,m}^{N} exp\left(\frac{-q^2 B_{n,m}(\tau)}{6}\right)$$

$$B_{n,m}(t) = |n-m|^{2\nu}l^2 + \frac{4R_e^2}{\pi^2}\sum_{p=0..\infty}\frac{A_p}{p^{2\nu+1}}\cos\left(\frac{\pi p n}{N}\right)\cos\left(\frac{\pi p m}{N}\right)(1-e^{-t/\tau_p}) \quad (4)$$

The internal motions of the chain are represented by relaxation modes with mode number *p* and characteristic mode relaxation times $\tau_p=p^{-3\nu}\tau_Z+\tau_{int}$. τ_Z is the characteristic Zimm time of the first mode with $\tau_Z = \eta R_e^3/\sqrt{3\pi}k_BT$ dependent on solvent viscosity η and end to end distance $R_e^2 = 6R_g^2 = l^2N^{2\nu}$. The parameter ν describes the polymer-solvent interaction and changes from 0.5 for a Θ-solvent to 0.6 for a good solvent with excluded volume. τ_{int} is the additional relaxation time due to internal friction[40]. The center of mass diffusion D_{Zimm} depends on the chain dimension $D_{Zimm}=k_BT/(\eta R_e)$. τ_Z can be rewritten for Θ-solvent in in relation to solvent friction and force constant as $\tau_Z = \xi_s/\kappa\ (N/\pi)^{3/2}/\sqrt{12}$. For internal friction the corresponding equation is $\tau_{int} = \xi_{int}/\kappa$. The mode amplitude factor A_p is in the standard ZIF model equal 1 but allows to examine modes suppression of e.g., low modes. At finite concentrations well below the overlap concentration c^* D_{Zimm} is modulated by the interaction between the chains as described by Akcasu[41]. Assuming decoupling of the intrachain configuration from the interchain structurefactor we may use the ZIF model to describe the chain dynamics and use the correction $D_{Zimm}=D_{t0}H/S(Q)$ with $H=H(Q\rightarrow\infty)$ for finite concentrations.

RESULTS

THE UNFOLDING TRANSITION

The thermal unfolding transition is examined by circular dichroism (CD) and dynamic light scattering (DLS) to establish conditions for a stable protein solution without aggregates at higher concentrations (50mg/ml) needed for later NSE measurements. CD determines the protein secondary structure while DLS results in the hydrodynamic radius of the protein as deduced from the diffusion coefficient with additional information about the formation of aggregates. We observe at pH7 that the unfolded protein is unstable and tends to aggregation. To stabilize the protein solution at the needed concentration we increased pH in order to increase the charge of Rnase for electrostatic stabilization. At pH2 no aggregates are observed.

The hydrodynamic radius increases from 20.1±0.4 Å in the native configuration to 24.1±0.4 Å in the unfolded state (see Figure 2 showing the respective unfolded fraction and Fig S1 in SI). CD at low concentrations (1mg/ml) shows that above pH4 an intermediate state occurs during thermal unfolding that is connected to partial unfolding of β-sheets with a transition temperature around 45°C while the α-helix and turn content remain constant[42,43]. The main transition occurs around 65° C. At pH2 the two transitions cannot be discriminated anymore and a seemingly two-state transition evolves (see Fig S2 and S3 in SI). The transition temperature shifts from 67°C at pH7 to 39°C at pH2. In the fully unfolded state about 70% of the protein are disordered and about 20% show residual α-helical or β-sheet structure as it is commonly observed also for IDP within the limits of the CD method. Only at pH2 we observe stable protein solution for longer times (several days) at temperatures up to 60°C where the protein is fully unfolded.

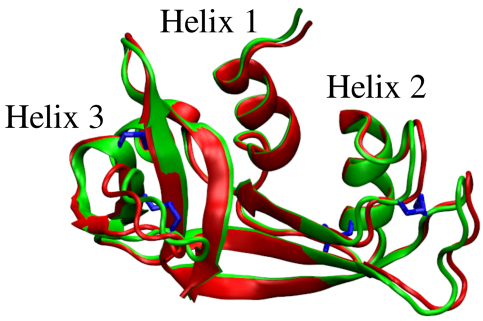

Figure 1 Structure of Rnase with 124 amino acids as cartoon image showing main secondary structure elements (green PDB 8RAT, red refined solution structure). Disulfide bonds (blue) are present between the cysteines 26-84, 58-110, 40-95, 65-72. Created using VMD[44].

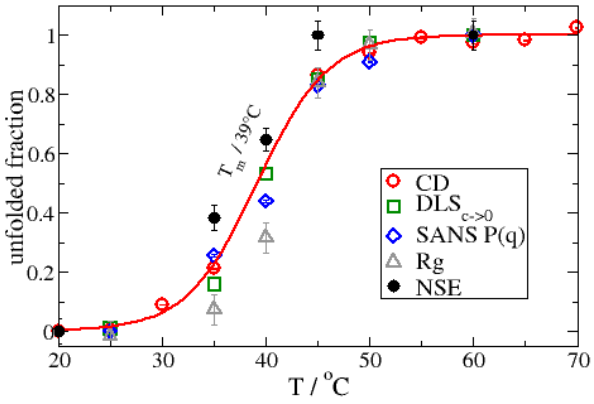

Figure 2: Protein denaturation curves showing the disordered (unfolded) fraction of RNase at pH2. To compare different methods all quantities S are normalized by the difference of states as $(S-S_{nativ})/(S_{disordered}-S_{nativ})$. A sigmoidal $\sim(1+\exp(-a(T-T_m)))^{-1}$ with the transition temperature T_m and the slope parameter *a=0.3 K^{-1}* as determined from a fit to the CD data is shown (black line). CD: disordered fraction from CD, DLS: R_h as extrapolated to concentration 0 from concentration series, SANS P(Q): unfolded fraction from fit with native and full unfolded SANS formfactors, R_g: R_g determined in Guinier range from SANS formfactors, NSE: fit parameter f_d from fit to NSE data.

DISULFIDE BONDS SHOW GEOMETRICAL RESTRICTION IN SAS

SANS/SAXS measurements allow the determination of the actual protein configuration including the hydration layer around the protein and determination of the structure factor. Figure 3 shows respective formfactors P(Q) as

extracted from concentration series and extrapolation to concentration 0 together with corresponding fits to adapted structural models. The native protein presents a configuration which is very close to the crystal structure found in PDB structure 8RAT[45]. For fitting the native structure was deformed along low frequency normal modes, a hydration layer with increased solvent density was added and the angle of helix-1 (which is sensitive to the SAXS peak at 0.5 Å^{-1}) was allowed to vary[46]. The simultaneous fit of SAX/SANS data with respective contrast resulted in the structure shown in Figure 1 (red) which is close to the crystal structure (green) with a hydration layer of 3Å thickness and an increase in solvent density of 3.2%. The helix-1 is only slightly shifted.

The unfolded protein at 60°C displays in the Kratky plot (Q vs. $Q^2P(Q)$) a characteristic peak with a following minimum and linear increase at high Q. A similar peak is already expected for polymer rings and denser branched polymer systems. For an unfolded Gaussian chain a plateau is expected[47]. To elucidate the role of the disulfide bonds and additional interactions affecting the configuration we performed coarse grained simulation within a bead and spring model (one bead per amino acid, with and without disulfide bonds) using the program SIMUFLEX[48] and calculated respective SAXS/SANS formfactors (for details see SI). The general appearance with a peak and minimum structure is clearly caused by the 4 disulfide bonds that lead to a geometrical restriction of the chain. The increase at larger Q is attributed to the linear dimension of the chain at short length scales resulting from the amino acid backbone stiffness. The radius of gyration for the disulfide containing simulation of R_g= 20.1Å from bead positions fits well to the observation from SANS at 60°C with 19.9±0.2 Å.

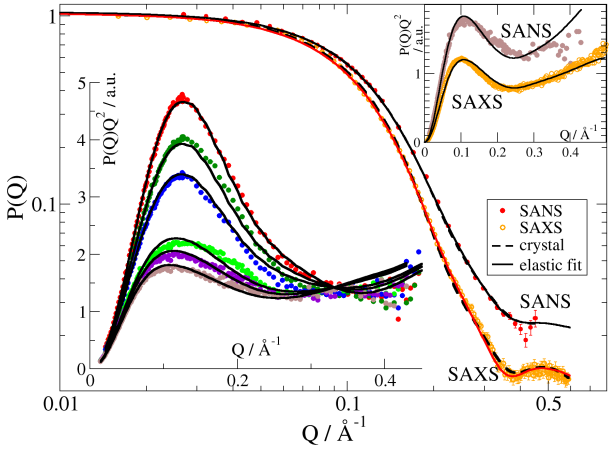

Figure 3. SAS formfactors as extracted from concentration series. 25°C: SAXS/SANS data of the native protein with lines as calculated from atomic refinement. Broken line is the 8RAT structure, solid line is the refinement. 60°C: Kratky plot of the disordered protein. Black lines show the ensemble average of 32 best fitting structures from the coarse grain modelling including disulfide bonds. 25°-60°C: SANS data in a Kratky plot at temperatures of 25°, 35°, 40°, 45°, 50°, and 60° Celsius showing the unfolding transition with corresponding fits of a two-state model.

Nevertheless, at larger Q deviations are observed compared to the average of the whole trajectory. A selection based on single best fits to SAXS/SANS data results in a good description of the respective formfactors as shown in Figure 3 for 60°. The best 8 configurations (see Fig S5 in SI) present mainly expanded cores and extended chain ends that may result from the 20 charged amino acids at pH2 leading to intra chain repulsion. The small difference between SAXS and SANS could be a result of the strong X-ray intensity (beamline instrument) introducing radicals even before radiation damage can be detected or even disulfide breakup is observed[49]. SANS introduces no radiation damage.

Formfactors in the transition region can be fitted assuming a two-phase transition with a linear combination of unfolded and folded formfactors. The fraction of unfolded chains is the only fit parameter. Fit results are shown in Figure 3 25°-60° and the resulting disordered fraction is presented in Figure 2 validating again the transition observed by CD. R_g as determined from a linear fit in the Guinier range shows an increase from 14.2±0.2 Å in the native state to 19.9±0.2 Å for the unfolded state. We note that the concentration scaled SANS and SAXS data after background correction show a nice overlap of the different concentrations at mid and high Q indicating that the configuration is not dependent on concentration.

Using the above formfactors $P(Q)$ the respective concentration dependent structure factor can be extracted using $S(Q)=I_c(Q)/c/P(Q)$. Figure 4 presents the respective structure factors for the concentration of the NSE experiments as measured by SANS. SAXS shows similar structure factors but with lower values at low Q (e.g. 0.15 lower for 60°C at lowest Q, data not shown) indicating a stronger repulsion which might be induced by additional radicals from radiation[49]. SANS structure factors are well described by the Hayter-Penfold (HP) structure factor describing charged spherical particles in a solvent containing screening ions[50]. The determining parameters are the particle radius, the surface potential and the screening length $\boldsymbol{\kappa}$ which depends on the ion concentration I as $\boldsymbol{\kappa}^{-2}=\boldsymbol{\varepsilon\varepsilon}_0 k_B T/2N_a e^2 I$ with temperature dependent permittivity $\boldsymbol{\varepsilon\varepsilon}_0$, thermal energy $k_B T$, Avogadro constant N_a and electron charge e. With a fixed effective ion concentration of I=28mM ($\boldsymbol{\kappa}\approx 5$Å) we observe a constant effective radius of 22.5(±1) Å and a surface potential $\boldsymbol{\Gamma}$ increasing from about 2.5 $k_B T$ to 9 $k_B T$ with rising temperature.

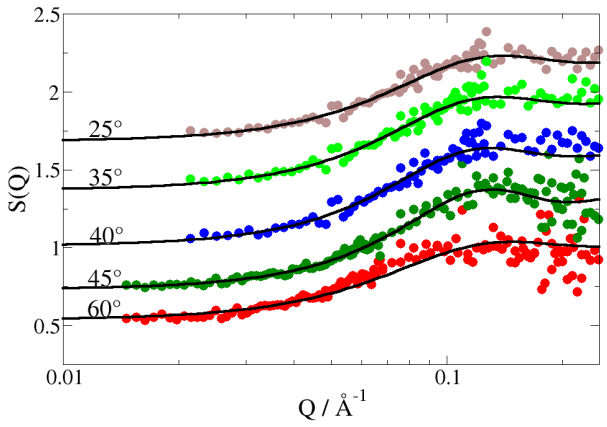

Figure 4 SANS structure factors for different temperatures as indicated. Lines represent fits using the Hayter-Penfold structure factor[50]. Data are shifted by 0.3 for better visibility.

It needs to be clarified that the observed structure factor is an effective two component structure factor between folded globular and unfolded chains. As both states are charged the HP structure factor seems to be a good approximation for this case. The configurational change during unfolding allows counterions present in the Stern layer to enter the effective volume of the disordered chain. This leads to a collapse of the charge compensation of the Stern layer but allows charge compensation by ion condensation on the chain. The net effect including the larger occupied volume seems to be an increase in the effective "surface" potential **Γ**.

FROM RIGID PROTEIN TO FLEXIBLE CHAIN DYNAMICS

To follow the unfolding transition on the intrinsic length and timescale scale of macromolecular motions we performed NSE measurements for 5 temperatures around the transition temperature of Rnase at pH2 as shown in Figure 5 and S6 (see SI). We note that the sample was always the same with stepwise increased temperature. To analyze the unfolding transition, we examine first the folded state and the unfolded state. The transition will be modeled again using a two-state model.

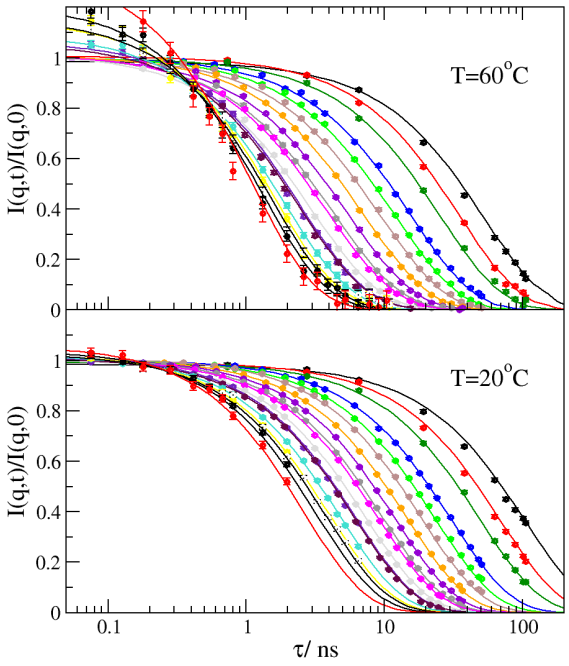

Figure 5 Intermediate scattering function as measured by NSE for Ribonuclease at temperatures as indicated. Lines correspond to the respective model fits as described in the text. Q values from 0.032Å^{-1}(black, right) to 0.22Å^{-1} (red, left) as also shown in Figure 6. Errors are of symbol size or smaller. The increased intensity for T=60˚C at high Q and short times is due to solvent incoherent scattering and the temperature mismatch of the background measurement (see SI Figure S6). This does not influence the results. Temperatures 35, 40, 45 ˚C are shown in SI Figure S6.

The effective diffusion coefficient $D_{eff}(Q)$ as extracted from the NSE data using a cumulant fit for T=20°C in the folded state is shown in Figure 6. We observe an increase towards low Q which is related to interparticle interactions and trends to the DLS value at lowest Q. At higher Q an increase related to the onset of protein rotational diffusion is observed[17]. To fit the full NSE spectra we use a model for rigid protein dynamics (see Methods) including translational and rotational diffusion with corrections for direct interactions and hydrodynamic interactions mediated by the solvent. While the relevant structure factor S(Q) can be measured H(Q) is calculated from the corresponding structure factor according to Beenakker and Mazur (see Methods). We fit a reduced effective hydrodynamic radius R_{eff} which comprises any reduced hydrodynamic interaction due to shape anisotropy or internal flexibility that might reduce the hydrodynamic interaction compared to a perfect hard sphere. The only free parameters during fitting are the translational diffusion D_{t0} and R_{eff} in the hydrodynamic function. The fit is shown in Figure 5 20°C while the resulting $D_{eff}(Q)$ (see equ. 2) is shown in Figure 6. We find that NSE spectra of native Rnase are in excellent agreement with the model calculations. The effective hydrodynamic radius R_{eff} is reduced from 13Å to 8Å demonstrating the influence of shape and protein softness. D_{t0}=8.5 Å^2/ns corresponds within 6% to the value calculated by HYDROPRO[51] using the refined Rnase PDB structure.

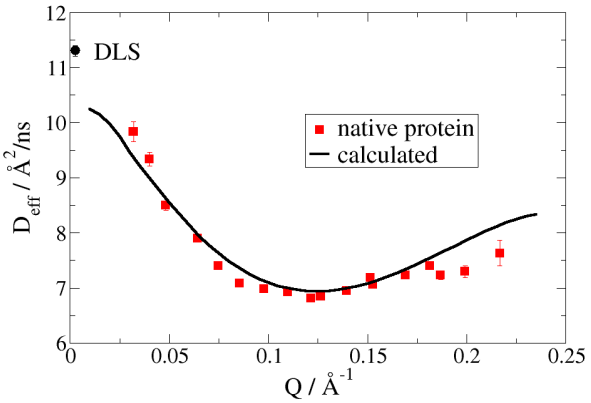

Figure 6 D_{eff} as extracted from a cumulant fit to NSE data of the native protein at T=20°C. The black line corresponds to $D_{eff}(Q)$ (see equ 2) from a fit to the full NSE spectra using the rigid protein dynamics model including S(Q) and H(Q) correction (see Methods). Additionally, the DLS value for the same concentration is given. We use S(Q) as fitted to 25°C data and adjusted the respective concentration in the HP structure factor.

The dynamics of the unfolded Rnase at 60°C is described by the ZIMM model with additional internal friction (ZIF). The center of mass diffusion D_{Zimm} needs again to be corrected for hydrodynamic and direct interactions like the previous case. Already preliminary measurements of viscosity and D_{Zimm} by DLS show that $H_\infty/H(Q\rightarrow 0)\approx 1$ with a constant hydrodynamic function describing the slowing down of self-diffusion with increasing concentration as it is expected for polymers (see table S1 in SI). The correction $D_{Zimm} \propto S(Q)^{-1}$ remains as a result of the charged disordered protein chain. To describe the unfolded protein, we use N=124 beads with a bond length l=3.8 Å corresponding to the amino acid

backbone in the ZIF model. The parameter ν is fixed to 0.53 to result in the observed R_g enclosing the effect of the 4 disulfide bonds. We limit the mode summation to p_{max}=10 as higher order modes contribute less than 0.01 to the signal. The fit results in an excellent description of the NSE spectra with D_{Zimm} and τ_{int} as the only fit parameters. The effect of these parameters on the model is demonstrated in figure S7 (see SI). The resulting D_{Zimm}=17.2 Å²/ns corresponds within 4% the value from DLS measurements with 17.9 Å²/ns. τ_{int} results in 8.7 ns which is about twice the corresponding relaxation time of the first Zimm mode τ_Z as shown in Figure 7. We tested also if the 4 disulfide bonds result in a suppression of the lowest modes (see Methods) but found no significant influence, suggesting that these intrachain links move more or less undistorted. The relaxation characteristics of the Zimm model relates to the hydrodynamic interaction between beads and leads to a mode relaxation time $\tau_p \sim p^{-3\nu}$. Since we found $\tau_i \cong 2\tau_Z$ the form of the Zimm spectrum is of very low impact and internal friction dominates already at the lowest modes. This insensitivity also reveals itself, if we insert the corresponding Rouse model with internal friction (RIF) that neglects hydrodynamic interaction between the beads[40] ($\tau_p \sim p^{-2}$) or an elastic chain model with internal friction (ECIF, as RIF with vanishing solvent friction $\xi_s \longrightarrow 0$ leading to $\tau_p \sim 0$). They result in slightly larger τ_{int} (RIF 9.4 ns, ECIF 13.1 ns) but fit equally well. The characteristic relaxation of the ECIF model corresponds to that of an ensemble of stiff chains with overdamped modes due to internal friction. The mode structure is the same as for ZIF/RIF.

To examine the NSE measurements in the transition region we used the two-state model already verified by our other measurements and use a linear combination of folded Rnase dynamics with dynamics of the disordered chain according to the disordered fraction f_d. For the H(Q)/S(Q) correction we use the experimental determined structure factor as an effective interaction between folded and disordered Rnase. Fit parameters are f_d, τ_{int} and D_{t0} for T=35, 40°C and f_d, τ_{int} and D_{Zimm} for T=45°C. The respective other value (D_{Zimm}, D_{t0}) is fixed to a viscosity scaled value based on T=20 and 60°C. Resulting fits are presented in Figure S6 35°C, 40°C and 45°C (see SI). We observe that the disordered fraction f_d (see Figure 2) is slightly larger than the disordered fraction measured by CD. This is an indication that also folded chain segments show a contribution to chain relaxation dynamics. The corresponding τ_{int} is shown in Figure 7 in comparison to τ_Z in an Arrhenius plot. For temperatures above 35°C a slightly stronger increase for τ_{int} compared to τ_Z is observed with $\tau_{int} \gtrsim 2\tau_Z$. While the latter is directly connected to the activation energy of solvent viscosity (water E_{act}≈15.7kJ/mol[52]) this is not obvious for internal friction. We find an activation energy of 33kJ/mol. Using the ECIF model we find a similar value of 28 kJ/mol verifying that the activation energy is related to the internal friction barrier.

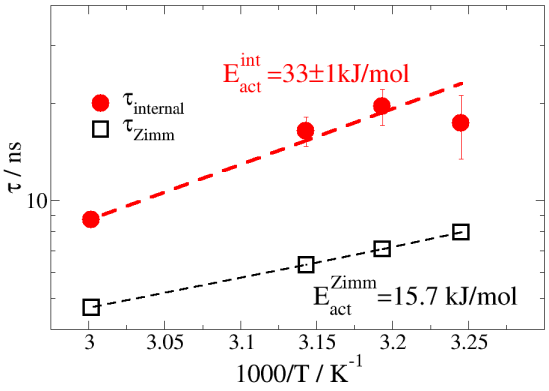

Figure 7 Internal relaxation time and Zimm time versus 1000/T in an Arrhenius plot.

DISCUSSION

The Rnase specific structure with 4 disulfide bonds acting as internal linker leads to a clear restriction of the protein conformation. The dynamic signature of the normal mode models is not influenced. This is at first surprising as a geometrical restriction might lead to suppression of modes if the strongest amplitudes are located at a linker or reduce the effective chain length. On the other hand, the linker only restricts movement to an additional collective character that coordinates larger segments like stars. These move coherently and thus contribute in a coherent manner to the observed scattering. At least the developing mode structure is close enough to the normal mode mode structure that differences are not significant at the observed length scales. This might change if the protein becomes larger and has more disulfide bonds that a domain structure evolves as in the case of chemically denatured unfolded bovine serum albumin[53].

For T=35°C we observe a small drop in τ_{int} compared to the Arrhenius expectation. As the disordered fraction is here smallest (CD 22%, NSE 38%) a larger error might be reasonable and the deviation is within errors. On the other hand, a structural reason might be considered in association with the increased f_d. Comparing the secondary structure trend at pH2 with pH7 measured by CD (see SI Fig S2) it is reasonable that at pH2 a kind of intermediate transition state is still present. Parts of the protein secondary structure may be folded or at least stabilized in a posttransitional state that cannot easily discriminated from a pretransitional state[54]. Posttransitional states represent structures closer to the native state allowing cooperative folding to the native configuration with smaller parts of the chain already prefolded. The reduced configurational freedom reduces rotations and dihedral motions resulting in a smaller effective τ_{int} compared to higher temperatures. A normal mode related model as ZIF/RIF/ECIF seems still to adequately describe this state which can be understood as follows: Higher order modes are suppressed by reduced local freedom but contribute in negligible amount to the observed large-scale dynamics. The lower order modes don't change their mode structure but show a significant reduced internal friction. This corresponds to rescaling the chain using larger (rigid) monomers keeping the spatial dimension (e.g. $R_e^2 = l^2 N$ for

RIF) constant which only affects the high mode cutoff. As most of the unfolded protein fraction is still in a disordered state the two-state assumption still describes the observed dynamics. This rescaling argument might also explain the larger dynamic contribution f_d to the disordered fraction in the NSE results. A small fraction of residual structure is always present representing structured segments in CD but still contribute to the observed dynamics.

The Zimm time τ_Z is here of same order of magnitude as the observed relaxation time due to internal friction as also observed by Soranno[11]. Relating both relaxation times to the friction per bead $\xi_{sol/int}$ (solvent and internal, respectively) with equal force constant κ and approximately equal relaxation times we find from the basic Langevin equation that the relative friction is $\xi_{int}/\xi_{sol} \approx (N/\pi)^{3/2}/(2\sqrt{3})$ which is >70 for Ribonuclease A with 124 amino acids. The friction per bead is dominated by internal friction which is even more important for higher modes p. For chains with lower internal friction (or reduced to the usage of osmolytes) the importance of solvent friction is related to the collective character of the lower normal modes. On the other hand, this highlights the role of internal friction for local chain motions due to torsion or local bending. Here the large sidechains of some amino acids might play an important role compared to Zimm like homopolymers (e.g. PEG) as already the sidechain excluded volume reduces configurational freedom. Decomposition of different contributions especially how neighboring sidechain character related to sidechain volume, hydrophilicity and charge influence activation energy and relaxation times may be possible using intrinsically disordered protein polymers with specifically designed amino acid composition[55].

The Zimm model, very successful to describe the dynamics of polymers, needs to be complemented by internal friction to the ZIF model as shown already earlier by Soranno or Stadler[11,15]. For ZIF the characteristic mode structure (amplitudes ~R_e) is unchanged and only the relaxation spectrum is modified. The dominating internal friction can be interpreted as a breakdown of the ZIF model and we observe overdamped motions in an ensemble of elastic chains spread in configurational space within the ECIF model. As $\tau_Z \sim R_e^3$ the collective character of Zimm might be recovered for longer chains, but on local scales or short chains internal friction is dominating and the elastic overdamped motions are similar to overdamped normal mode motions of structured proteins with hinge or shear domain motions[46]. For RIF and ZIF model internal friction is a correction from the original Rouse and Zimm dynamic models. For IDP under natural conditions internal friction dominates while solvent friction and hydrodynamic interactions are smaller corrections. The notable advantage of models as ZIF/RIF/ECIF over models requiring explicit configurations (elastic normal mode analysis and at least a minimal ensemble average) is that the ensemble average is implicitly included. On the other hand, if sequence details of the secondary structure become more important explicit models taking secondary structure into account can be advantageous.

The Arrhenius behavior of simple liquid viscosity is connected to the reconfiguration of molecules in the cage of next neighbors (neglecting here the more complex structure of water)[56]. The activation energy is related to the free energy for escaping this cage. τ_Z as the time of the slowest and largest mode of a collective movement of the chain is coupled to the viscosity of the solvent resulting in a solvent dependent activation energy. The slowing down of mode relaxation times compared to water diffusion is again a result of the collective character of low modes. Internal friction is related to local intrachain interactions as dihedral angle rotation, intrachain and sidechain collisions. While also sidechain movements are influenced by friction with the solvent this contribution seems to be small according to the above friction per bead argument. The observed activation energy of 33 kJ/mol for τ_{int} may be interpreted as the roughness of the local energy landscape of intrachain interactions. This value might also be related to the peptide rotational barrier for NC^α bonds of about 66kJ/mol and $C^\alpha C$ bond of about 25kJ/mol[57]. While the NC^α bonds are assumed to be stiff, the $C^\alpha C$ barrier fits reasonably well to our observation.

Finally, we may compare the slowest mode relaxations times of 10-20 ns of the unfolded chain to folding/unfolding rates measured by other techniques. Torrent et al. used T-jump experiments for Ribonuclease A at pH5 resulting in several milliseconds unfolding time. Fierz et al. used triplet-triplet energy transfer to observe α-helix formation times of 400ns (at 5°C in H_2O, ≈210ns at 40°C in D_2O scaled by viscosity). Recalling that the dominating modes are equivalent to overdamped elastic modes of an ensemble of disordered configurations we may conclude that we observe mainly the faster equilibrium dynamics of disordered chains as the prerequisite for slower chain reconfiguration and folding.

CONCLUSIONS

In the present paper we examined the internal dynamics of the unfolded amino acid chain of Ribonuclease A in different states of the unfolding process to enlighten the role of internal friction onto protein chain dynamics. At first it needs to be recognized that the two-state transition model observed using integral methods as DLS and CD is also observed in dynamics with rigid folded and flexible disordered protein conformations. The disordered fraction contributing to dynamics is systematically larger than the disordered fraction obtained from static methods as CD. The internal dynamics of the protein chain is dominated by internal friction between amino acids and is rather insensitive to the details of the mode structure as ZIF/RIF/ECIF models are all compatible with the observed dynamics. It is questionable if these models are superior over ensemble averaged elastic normal mode analysis of IDP or during the protein folding/unfolding.

Supporting Information

The Supporting Information is available free of charge on the ACS Publications website.

DLS, CD Spectroscopy, DLS and viscosity measurement results, Coarse Grain Simulation results, NSE Spectra (SupportingInfo.pdf)

AUTHOR INFORMATION

Corresponding Author

* ra.biehl@fz-juelich.de

Author Contributions

‡These authors contributed equally.

Notes

The authors declare no competing financial interest.

This research did not receive any specific grant from funding agencies in the public, commercial, or not-for-profit sectors.

ACKNOWLEDGMENT

This work is based on experiments performed at the ILL, Grenoble, France, EMBL at DESY, Hamburg, Germany and at the Heinz Maier-Leibnitz Zentrum (MLZ), Garching, Germany. We thank B. Hoffmann for help during sample preparation and T. Rosenkranz for help during CD spectroscopy measurements.

REFERENCES

(1) Fischer, E. Einfluss Der Configuration Auf Die Wirkung Der Enzyme. *Berichte der Dtsch. Chem. Gesellschaft* **1894**, *27* (3), 2985–2993. https://doi.org/10.1002/cber.18940270364.

(2) Dyson, H. J.; Wright, P. E. Intrinsically Unstructured Proteins and Their Functions. *Nat Rev Mol Cell Biol* **2005**, *6* (3), 197–208. https://doi.org/10.1038/nrm1589.

(3) Uversky, V. N. Natively Unfolded Proteins: A Point Where Biology Waits for Physics. *Protein Sci.* **2002**, *11* (4), 739–756.

(4) Midtgaard, S. R.; Darwish, T. A.; Pedersen, M. C.; Huda, P.; Larsen, A. H.; Jensen, G. V.; Kynde, S. A. R.; Skar-Gislinge, N.; Nielsen, A. J. Z.; Olesen, C.; Blaise, M.; Dorosz, J. J.; Thorsen, T. S.; Venskutonytė, R.; Krintel, C.; Møller, J. V.; Frielinghaus, H.; Gilbert, E. P.; Martel, A.; Kastrup, J. S.; Jensen, P. E.; Nissen, P.; Arleth, L. Invisible Detergents for Structure Determination of Membrane Proteins by Small-Angle Neutron Scattering. *FEBS J.* **2018**, *285* (2), 357–371. https://doi.org/10.1111/febs.14345.

(5) Gunasekaran, K.; Tsai, C.-J.; Kumar, S.; Zanuy, D.; Nussinov, R. Extended Disordered Proteins: Targeting Function with Less Scaffold. *Trends Biochem. Sci.* **2003**, *28* (2), 81–85. https://doi.org/10.1016/S0968-0004(03)00003-3.

(6) Dill, K. A.; MacCallum, J. L. The Protein-Folding Problem, 50 Years On. *Science*. American Association for the Advancement of Science November 23, 2012, pp 1042–1046. https://doi.org/10.1126/science.1219021.

(7) Malhotra, P.; Udgaonkar, J. B. How Cooperative Are Protein Folding and Unfolding Transitions? *Protein Science*. Wiley-Blackwell 2016, pp 1924–1941. https://doi.org/10.1002/pro.3015.

(8) Cellmer, T.; Henry, E. R.; Hofrichter, J.; Eaton, W. A. Measuring Internal Friction of an Ultrafast-Folding Protein. *Proc. Natl. Acad. Sci. U. S. A.* **2008**, *105* (47), 18320–18325. https://doi.org/10.1073/pnas.0806154105.

(9) Ansari, A.; Jones, C. M.; Henry, E. R.; Hofrichter, J.; Eaton, W. A. The Role of Solvent Viscosity in the Dynamics of Protein Conformational Changes. *Science (80-.).* **1992**, *256* (5065), 1796–1798. https://doi.org/10.1126/science.1615323.

(10) Pradeep, L.; Udgaonkar, J. B. Diffusional Barrier in the Unfolding of a Small Protein. *J. Mol. Biol.* **2007**, *366* (3), 1016–1028. https://doi.org/10.1016/j.jmb.2006.11.064.

(11) Soranno, A.; Buchli, B.; Nettels, D.; Cheng, R. R.; Müller-Späth, S.; Pfeil, S. H.; Hoffmann, A.; Lipman, E. a; Makarov, D. E.; Schuler, B. Quantifying Internal Friction in Unfolded and Intrinsically Disordered Proteins with Single-Molecule Spectroscopy. *Proc. Natl. Acad. Sci. U. S. A.* **2012**, *109* (44), 17800–17806. https://doi.org/10.1073/pnas.1117368109.

(12) Kramers, H. A. Brownian Motion in a Field of Force and the Diffusion Model of Chemical Reactions. *Physica* **1940**, *7* (4), 284–304. https://doi.org/10.1016/S0031-8914(40)90098-2.

(13) Doi, M.; Edwards, S. F. *The Theory of Polymer Dynamics*; Birman, J., Edwards, S. F., LLewellyn Smith, C. H., Rees, M., Eds.; Oxford University Press, USA: Oxford, 1988. https://doi.org/10.1016/S1359-0286(96)80106-9.

(14) Soranno, A.; Holla, A.; Dingfelder, F.; Nettels, D.; Makarov, D. E.; Schuler, B. Integrated View of Internal Friction in Unfolded Proteins from Single-Molecule FRET, Contact Quenching, Theory, and Simulations. *Proc. Natl. Acad. Sci. U. S. A.* **2017**, *114* (10), E1833–E1839. https://doi.org/10.1073/pnas.1616672114.

(15) Stadler, A. M.; Stingaciu, L.; Radulescu, A.; Holderer, O.; Monkenbusch, M.; Biehl, R.; Richter, D. Internal Nanosecond Dynamics in the Intrinsically Disordered Myelin Basic Protein. *J. Am. Chem. Soc.* **2014**, *136* (19), 6987–6994. https://doi.org/10.1021/ja502343b.

(16) Abyzov, A.; Salvi, N.; Schneider, R.; Maurin, D.; Ruigrok, R. W. H.; Jensen, M. R.; Blackledge, M. Identification of Dynamic Modes in an Intrinsically Disordered Protein Using Temperature-Dependent NMR Relaxation. *J. Am. Chem. Soc.* **2016**, *138* (19), 6240–6251. https://doi.org/10.1021/jacs.6b02424.

(17) Biehl, R.; Monkenbusch, M.; Richter, D. Exploring Internal Protein Dynamics by Neutron Spin Echo Spectroscopy. *Soft Matter* **2011**, *7* (4), 1299–1307. https://doi.org/10.1039/C0SM00683A.

(18) Neira, J. L.; Rico, M. Folding Studies on Ribonuclease A, a Model Protein. *Folding and Design*. Cell Press February 1, 1997, pp R1–R11. https://doi.org/10.1016/S1359-0278(97)00001-1.

(19) Krężel, A.; Bal, W. A Formula for Correlating PKa Values Determined in D2O and H2O. *J. Inorg. Biochem.* **2004**, *98* (1), 161–166. https://doi.org/10.1016/j.jinorgbio.2003.10.001.

(20) Sreerama, N.; Woody, R. W. Estimation of Protein Secondary Structure from Circular Dichroism Spectra: Comparison of CONTIN, SELCON, and CDSSTR Methods with an Expanded Reference Set. *Anal. Biochem.* **2000**, *287* (2), 252–260. https://doi.org/10.1006/abio.2000.4880.

(21) Provencher, S. W. CONTIN: A General Purpose Constrained Regularization Program for Inverting Noisy Linear Algebraic and Integral Equations. *Comput. Phys. Commun.* **1982**, *27* (3), 229–242. https://doi.org/10.1016/0010-4655(82)90174-6.

(22) Roessle, M. W.; Klaering, R.; Ristau, U.; Robrahn, B.; Jahn, D.; Gehrmann, T.; Konarev, P.; Round, A.; Fiedler, S.; Hermes, C.; Svergun, D. Upgrade of the Small-Angle X-Ray Scattering Beamline X33 at the European Molecular Biology Laboratory, Hamburg. *J. Appl. Crystallogr.* **2007**, *40* (s1), s190–s194. https://doi.org/10.1107/S0021889806055506.

(23) Radulescu, A.; Pipich, V.; Frielinghaus, H.; Appavou, M.-S. KWS-2, the High Intensity / Wide Q -Range Small-Angle Neutron Diffractometer for Soft-Matter and Biology at FRM II. *J. Phys. Conf. Ser.* **2012**, *351* (1), 012026. https://doi.org/10.1088/1742-6596/351/1/012026.

(24) Pedersen, J. S.; Posselt, D.; Mortensen, K. Analytical Treatment of the Resolution Function for Small-Angle Scattering. *J. Appl. Crystallogr.* **1990**, *23* (4), 321–333.

(25) V. Pipich. QtiKWS http://qtisas.com/doku.php?id=start (accessed Feb 6, 2020).

(26) Petoukhov, M. V.; Franke, D.; Shkumatov, A. V.; Tria, G.; Kikhney, A. G.; Gajda, M.; Gorba, C.; Mertens, H. D. T.; Konarev, P. V.; Svergun, D. I. New Developments in the ATSAS Program Package for Small-Angle Scattering Data Analysis. *J. Appl. Crystallogr.* **2012**, *45* (2), 342–350. https://doi.org/10.1107/S0021889812007662.

(27) Biehl, R. Jscatter, a Program for Evaluation and Analysis of Experimental Data. *PLoS One* **2019**, *14* (6), e0218789. https://doi.org/10.1371/JOURNAL.PONE.0218789.

(28) Hinsen, K. The Molecular Modeling Toolkit: A New Approach to Molecular Simulations. *J. Comput. Chem.* **2000**, *21* (2), 79–85. https://doi.org/10.1002/(SICI)1096-987X(20000130)21:2<79::AID-JCC1>3.0.CO;2-B.

(29) Biehl, R.; Richter, D. Slow Internal Protein Dynamics in Solution. *J. Phys. Condens. Matter* **2014**, *26* (50), 503103. https://doi.org/10.1088/0953-8984/26/50/503103.

(30) Lindsay, H. M.; Klein, R.; Weitz, D. A.; Lin, M. Y.; Meakin, P. Effect of Rotational Diffusion on Quasielastic Light Scattering from Fractal Colloid Aggregates. *Phys. Rev. A* **1988**, *38* (5), 2614–2626. https://doi.org/10.1103/PhysRevA.38.2614.

(31) de la Torre, J. G.; Huertas, M. L.; Carrasco, B.; de la Torre, J. Calculation of Hydrodynamic Properties of Globular Proteins from Their Atomic-Level Structure. *Biophys. J.* **2000**, *78* (2), 719–730. https://doi.org/10.1016/S0006-3495(00)76630-6.

(32) Degiorgio, V.; Piazza, R.; Jones, R. B. Rotational Diffusion in Concentrated Colloidal Dispersions of Hard Spheres. *Phys. Rev. E* **1995**, *52* (3), 2707–2717. https://doi.org/10.1103/PhysRevE.52.2707.

(33) Mazur, P. Many-Sphere Hydrodynamic Interactions. *Faraday Discuss. Chem. Soc.* **1987**, *83* (0), 33. https://doi.org/10.1039/dc9878300033.

(34) Banchio, A. J.; Gapinski, J.; Patkowski, A.; Haussler, W.; Fluerasu, A.; Sacanna, S.; Holmqvist, P.; Meier, G.; Lettinga, M. P.; Nagele, G. Many-Body Hydrodynamic Interactions in Charge-Stabilized Suspensions. *Phys. Rev. Lett.* **2006**, *96* (13), 138303. https://doi.org/10.1103/PhysRevLett.96.138303.

(35) Gapinski, J.; Wilk, A.; Patkowski, A.; Haussler, W.; Banchio, A. J.; Pecora, R.; Nagele, G. Diffusion and Microstructural Properties of Solutions of Charged Nanosized Proteins: Experiment versus Theory. *J. Chem. Phys.* **2005**, *123* (5), 54708. https://doi.org/10.1063/1.1996569.

(36) Kotlarchyk, M.; Chen, S.-H. Analysis of Small Angle Neutron Scattering Spectra from Polydisperse Interacting Colloids. *J. Chem. Phys.* **1983**, *79* (5), 2461. https://doi.org/10.1063/1.446055.

(37) Riese, D. O.; Wegdam, G. H.; Vos, W. L.; Sprik, R.; Fenistein, D.; Bongaerts, J. H. H.; Grübel, G. Effective Screening of Hydrodynamic Interactions in Charged Colloidal Suspensions. *Phys. Rev. Lett.* **2000**, *85* (25), 5460–5463.

(38) Beenakker, C. W. J.; Mazur, P. Diffusion of Spheres in a Concentrated Suspension II. *Phys. A Stat. Mech. its Appl.* **1984**, *126* (3), 349–370. https://doi.org/10.1016/0378-4371(84)90206-1.

(39) Genz, U.; Klein, R. Collective Diffusion of Charged Spheres in the Presence of Hydrodynamic Interaction. *Phys. A Stat. Mech. its Appl.* **1991**, *171* (1), 26–42. https://doi.org/https://doi.org/10.1016/0378-4371(91)90355-G.

(40) Cheng, R. R.; Hawk, A. T.; Makarov, D. E. Exploring the Role of Internal Friction in the Dynamics of Unfolded Proteins Using Simple Polymer Models. *J. Chem. Phys.* **2013**, *138* (7), 074112. https://doi.org/10.1063/1.4792206.

(41) Akcasu, A. Z. Temperature and Concentration Dependence of Diffusion Coefficient in Dilute Solutions. *Polymer (Guildf).* **1981**, *22* (9), 1169–1180. https://doi.org/10.1016/0032-3861(81)90129-4.

(42) Barone, G.; Catanzano, F.; Vecchio, P. Del; Giancola, C.; Graziano, G. Thermodynamics of Protein Stability: A Family of Ribonucleases. *Pure Appl. Chem.* **1997**, *69* (11), 2307–2313. https://doi.org/10.1351/pac199769112307.

(43) Stelea, S. D.; Pancoska, P.; Benight, A. S.; Keiderling, T. A. Thermal Unfolding of Ribonuclease A in Phosphate at Neutral PH: Deviations from the Two-State Model. *Protein Sci.* **2001**, *10* (5), 970–978. https://doi.org/10.1110/ps.47101.

(44) Humphrey, W.; Dalke, A.; Schulten, K. VMD: Visual Molecular Dynamics. *J. Mol. Graph.* **1996**, *14* (1), 33–38. https://doi.org/10.1016/0263-7855(96)00018-5.

(45) Tilton, R. F.; Dewan, J. C.; Petsko, G. A. Effects of Temperature on Protein Structure and Dynamics: X-Ray Crystallographic Studies of the Protein Ribonuclease-A at Nine Different Temperatures from 98 to 320 K. *Biochemistry* **1992**, *31* (9), 2469–2481. https://doi.org/10.1021/bi00124a006.

(46) Inoue, R.; Biehl, R.; Rosenkranz, T.; Fitter, J.; Monkenbusch, M.; Radulescu, A.; Farago, B.; Richter, D. Large Domain Fluctuations on 50-Ns Timescale Enable Catalytic Activity in Phosphoglycerate Kinase. *Biophys. J.* **2010**, *99* (7), 2309–2317. https://doi.org/10.1016/j.bpj.2010.08.017.

(47) Hammouda, B. SANS from Homogeneous Polymer Mixtures: A Unified Overview. *Advances in Polymer Science*. Springer-Verlag: Berlin/Heidelberg 1993, pp 86–133. https://doi.org/10.1007/bfb0025862.

(48) de la Torre, J. G.; Cifre, J. G. H.; Ortega, Á.; Schmidt, R. R.; Fernandez, M. X.; Sánchez, H. E. P.; Pamies, R. SIMUFLEX : Algorithms and Tools for Simulation of the Conformation and Dynamics of Flexible Molecules and Nanoparticles in Dilute Solution. *J. Chem. Theory Comput.* **2009**, *5* (10), 2606–2618. https://doi.org/10.1021/ct900269n.

(49) Kuwamoto, S.; Akiyama, S.; Fujisawa, T. Radiation Damage to a Protein Solution, Detected by Synchrotron X-Ray Small-Angle Scattering: Dose-Related Considerations and Suppression by Cryoprotectants. *J. Synchrotron Radiat.* **2004**, *11* (6), 462–468. https://doi.org/10.1107/S0909049504019272.

(50) Hayter, J. B.; Penfold, J. An Analytic Structure Factor for Macroion Solutions. *Mol. Phys.* **1981**, *42* (1), 109–118. https://doi.org/10.1080/00268978100100091.

(51) Ortega, A.; Amorós, D.; Torre, J. de la; de la Torre, J. G. Prediction of Hydrodynamic and Other Solution Properties of Rigid Proteins from Atomic- and Residue-Level Models. *Biophys. J.* **2011**, *101* (4), 892–898. https://doi.org/10.1016/j.bpj.2011.06.046.

(52) Messaâdi, A.; Dhouibi, N.; Hamda, H.; Belgacem, F. B. M.; Adbelkader, Y. H.; Ouerfelli, N.; Hamzaoui, A. H. A New Equation Relating the Viscosity Arrhenius Temperature and the Activation Energy for Some Newtonian Classical Solvents. *J. Chem.* **2015**, *2015*, 163262. https://doi.org/10.1155/2015/163262.

(53) Ameseder, F.; Radulescu, A.; Holderer, O.; Falus, P.; Richter, D.; Stadler, A. M. Relevance of Internal Friction and Structural Constraints for the Dynamics of Denatured Bovine Serum Albumin. *J. Phys. Chem. Lett.* **2018**, *9* (10), 2469–2473. https://doi.org/10.1021/acs.jpclett.8b00825.

(54) Dokholyan, N. V.; Li, L.; Ding, F.; Shakhnovich, E. I. Topological Determinants of Protein Folding. *Proc. Natl. Acad. Sci. U. S. A.* **2002**, *99* (13), 8637–8641. https://doi.org/10.1073/pnas.122076099.

(55) Quiroz, F. G.; Chilkoti, A. Sequence Heuristics to Encode Phase Behaviour in Intrinsically Disordered Protein Polymers. *Nat. Mater.* **2015**, *14* (11), 1164–1171. https://doi.org/10.1038/nmat4418.

(56) Bird, R. B. (Robert B.; Stewart, W. E.; Lightfoot, E. N. Transport Phenomena, (2nd Edition). J. Wiley 2002, p 895.

(57) Basharov, M. A. The Internal Rotational Barriers about NCα and CαC Backbone Bonds of Polypeptides. *European Biophysics Journal*. Springer January 3, 2012, pp 53–61. https://doi.org/10.1007/s00249-011-0757-5.

SYNOPSIS TOC